RSC Advances

This is an *Accepted Manuscript*, which has been through the Royal Society of Chemistry peer review process and has been accepted for publication.

Accepted Manuscripts are published online shortly after acceptance, before technical editing, formatting and proof reading. Using this free service, authors can make their results available to the community, in citable form, before we publish the edited article. This *Accepted Manuscript* will be replaced by the edited, formatted and paginated article as soon as this is available.

You can find more information about *Accepted Manuscripts* in the Information for Authors.

Please note that technical editing may introduce minor changes to the text and/or graphics, which may alter content. The journal's standard Terms & Conditions and the Ethical guidelines still apply. In no event shall the Royal Society of Chemistry be held responsible for any errors or omissions in this *Accepted Manuscript* or any consequences arising from the use of any information it contains.

ROYAL SOCIETY OF CHEMISTRY

www.rsc.org/advances

RSC Advances

RSCPublishing

ARTICLE

Photo-crosslinked hierarchically honeycomb-patterned/macroporous scaffolds of calcium phosphate cement promote MC3T3-E1 cell functions

X. H. Wu,[a] Z. Y. Wu[b] , J Qian[b*], Y.G.Yan[c] , J. Wei [b], H. Li[c] J. C. Su[d*]

Cite this: DOI: 10.1039/xoxxoooooox

Received ooth January 2012,
Accepted ooth January 2012

DOI: 10.1039/xoxxoooooox

www.rsc.org/

The advanced technology has enabled us to investigate cell functions on biomimetic honeycomb films or macroporous inorganic scaffolds to tentatively seek more powerful engineered biomaterials for bone regeneration. However, to date, the cell functions on honeycomb-patterned 3-dimensional scaffolds have not been studied. Herein, we report a facile and novel approach to fabricating photo-crosslinked hierarchically honeycomb-patterned/macroporous calcium phosphate cement (CH-CPC) scaffolds and their biological impact on MC3T3-E1 cells. The CH-CPC scaffolds together with controls, photo-crosslinked calcium phosphate cement scaffolds without honeycomb pores (CW-CPC) and calcium phosphate cement (CPC) scaffolds, were characterized by scanning electron microscopy (SEM), X-ray diffraction (XRD), energy dispersive spectroscopy (EDS), gel fraction measurement, thermogravimetric analysis (TGA), Brunauer-Emmer-Teller (BET) test, and mechanical test. The CH-CPC scaffolds were fully covered with a honeycomb layer with a pore diameter of 1.5~3.7 μm on the scaffold surface and the inside of CH-CPC scaffolds was also covered with a honeycomb layer, but with poorer coverage and regularity in term of pore size. The crosslinked networks in CW-CPC and CH-CPC scaffolds enhanced their compressive strength. The surface area and water adsorption in CH-CPC scaffolds were significantly higher than CPC and CW-CPC scaffolds due to the formation of honeycomb pores, which also promoted the fibronectin (FN) adsorption on CH-CPC scaffolds. The MC3T3-E1 cells were seeded on these scaffolds to study the cell response. The results clearly suggested that, in comparison with CPC and CW-CPC scaffolds, cell adhesion, spreading, proliferation, and differentiation were enhanced on CH-CPC scaffolds.

RSC Advances Accepted Manuscript

Introduction

A large number of people worldwide suffer bone loss due to injury, disease, and infection, and the treatment generally requires the regeneration of new bone.[1] Yet each patient has limited bone resource for grafting. The demand for synthetic bone substitutes is highly needed, but unmet. The ideal substitutes for bone regeneration have several characteristics, such as biocompatibility, biodegradation, suitable mechanical property, and bioactivity. The biomaterials currently available for bone repair are far from optimal. CPC with excellent biocompatibility and osteoconductivity has drawn increasing attention, since reported in 1986.[2, 3] CPC resembles the composition of natural bone and can gradually degrade to induce the formation of hydroxylapatite (HA) in *vivo*, which promotes resorption and replacement by newly generated bone.[3] However, the resorption and replacement rates are still not satisfactory. Recently, it is suggested that porous scaffolds with a high porosity and 3-dimensional interconnected pore structures are desired due to the enhanced permeability and diffusion properties for both cell penetration and the effective vascularization of the ingrowth tissue, and as well as improved degradation.[4] Porous CPC scaffolds with macro-pores ranging from 400 to 500 μm have been extensively investigated as bone substitutes and performed attractive biocompatibility, bioactivity, biodegradation, and osteoconductivity.[3, 5] Nonetheless, the generation of macro-pores in CPC scaffolds, in turn, has weakened the mechanical performance significantly compared with these CPC scaffolds without macro-pores, which prevents their promising application in clinical treatment.

Recently, honeycomb polymeric films with uniform pore size ranging from 1 μm to 20 μm have been developed to mimic the surface feature of basement membranes in vertebrate body, which

have complex topographies,[6-10] such as pores, grooves, wells, and pillars at micro-/nano-scale, and utilized to tune cell functions due to the fact that adherent cells can react to topography through "contact guidance".[6-8, 11-14] The cell behavior on honeycomb films was demonstrated to be cell type-dependent. Osteoblast cells were also evaluated on honeycomb films in terms of cell adhesion, spreading, proliferation, and differentiation, which were prominently enhanced by honeycomb pores, especially smaller ones.[7, 9] However, the honeycomb polymeric films have been restricted on flat substrata and they generally lack good mechanical performance, which strongly limits their application for bone repair. To date, there is no literature reporting the cell response to honeycomb pores combined with 3-dimensional architecture.

Even though the emerging advanced techniques have provided great approaches to fabricating honeycomb films and porous scaffolds, and enabled us to investigate the cell functions on either honeycomb films or porous scaffolds, scientists have not yet developed an useful modality to fabricate porous scaffolds, the surfaces including walls, valleys, and ridges of which are patterned with honeycomb pores, and studied their influence on cells. In earlier studies, the honeycomb-patterned specimens with hierarchal surface features have been fabricated using transmission electron microscopy (TEM) grids bearing specific morphologies, such as hexagonal, groove, square, and even particles including golf balls, doughnuts, and hollow pockets as templates. [15-18] Inspired by this finding, in this study we report a novel modality to fabricate CPC scaffolds (pore size: ~500 μm) with honeycomb pores of poly(L-lactide) triacrylate (PLLATA) fully formed on macro-pore walls, valleys, and ridges of CPC scaffolds. Moreover, the honeycomb PLLATA will be further photo-crosslinked to stabilize the structure, which is expected to enhance the mechanical performance of CPC scaffolds. Poly(L-lactide) (PLLA) has received extensive investigation and wide applications in biomedical field due to its excellent biocompatibility, biodegradability, and low immunogenicity.[19, 20] We hypothesize that the combination of crosslinked honeycomb polymeric PLLATA and CPC scaffolds will render these novel scaffolds several attractive advantages over the CPC scaffolds. First, the crosslinked networks available in the novel scaffolds may increase the mechanical performance of CPC scaffolds and also stabilize the physical structure. Second, the formation of honeycomb pores might improve the porosity of scaffolds and change the degradation kinetics. Third, as demonstrated earlier, the honeycomb films promoted MC3T3-E1 cell functions including adhesion, proliferation, and differentiation, these novel scaffolds might support better cell functions than CPC scaffolds.

Experimental Section

Preparation of CPC scaffolds

CPC scaffolds were fabricated using a particulate-leaching method as reported previously.[2, 3] The CPC powders (Shanghai Rebone Biomaterials Co., Ltd, Shanghai, China), sodium chloride particles (diameter: 400~500 μm), and saturated salt water were mixed thoroughly at a mass ratio of 1:3:2. The mixture then was placed in stainless steel molds and molded under a pressure of 2 MPa, followed by incubation at 37 °C and 100% relative humidity (RH). The sodium chloride particles as porogens were leached out in deionized water. The white sponge-like CPC scaffolds (ϕ6 × 6 mm) were obtained after completely dried in vacuum.

Fabrication of CW-CPC and CH-CPC scaffolds

The CH-CPC scaffolds were prepared via breath-figure method partially referred to previous reports.[7, 9] PLLATA (Mn = 18,372 g mol^{-1}, Mw = 21, 890 g mol^{-1}) was synthesized through ring-opening polymerization of L-lactide monomer at 130 °C overnight with $Sn(Oct)_2$ as the catalyst and 1,1,1-tris(hydroxymethyl) propane (TMP) as the initiator according to the previous procedure.[21] PLLATA and photo-initiator, phenyl bis(2,4,6-trimethyl benzoyl) phosphine oxide (BAPO), were thoroughly dissolved in dichloromethane (DCM) at a concentration of 0.05 g mL^{-1} and 0.5 mg mL^{-1}, respectively. As shown in Scheme 1, the CPC scaffold, hanged with a needle in the center, was immersed in PLLATA/BAPO solution. The CPC scaffold was pulled up slowly at a speed of ~0.5 mm min^{-1} when the moist airflow (100 mL min^{-1}), generated from flowing through distilled water, was applied. Afterwards, the scaffold was crosslinked by exposure to UV light for 30 min and completely dried under reduced pressure overnight. The CW-CPC scaffold was prepared via the same procedure, but without the application of moist airflow.

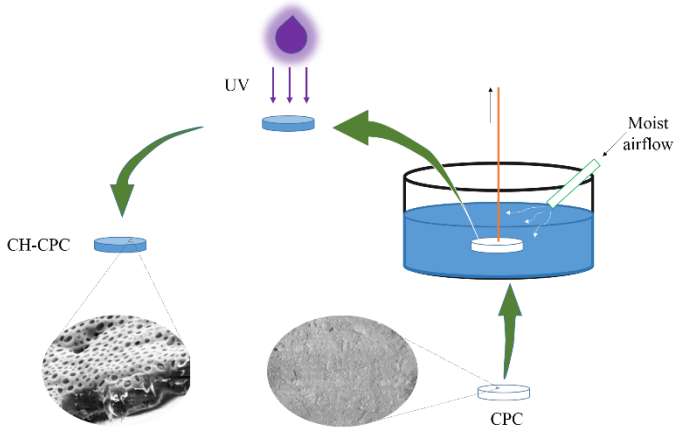

Scheme 1. Schematical illustration for fabricating CH-CPC scaffolds.

Characterizations

The morphology of scaffolds was observed using SEM (JEOL-6360, Japan) at an accelerating voltage of 10 kV after sputter-coated with gold-palladium. XRD (Rigaku Multiflex) was employed to analyze the phase composition of scaffolds with Cu Kα radiation at 40 kV and 100 mA. TGA was performed on a TGA2050 thermogravimetric analyzer (TA Instruments Inc., USA) at a heating rate of 20 °C min^{-1} from 22 °C to 800 °C. To measure the gel fractions, the weight of the original scaffold was recorded as W_o. After the formation of photo-crosslinked PLLATA layer, the weight of the CH-CPC scaffold or the CW-CPC scaffold was measured as W_p. The photo-crosslinked sample was then immersed in excessive DCM for 3 days, followed by drying under reduced pressure for 1 day and weighing as W_d. The gel fraction was calculated using $(W_d - W_o)/(W_p - W_o) \times 100\%$. The compressive strengths of scaffolds were measured at a loading rate of 1 mm min^{-1} using a mechanical testing machine (HY-0230, Shanghai, China) at room temperature. The porosity of the scaffolds was measured using the Archimedes method in deionized water. The Brunauer-Emmer-Teller (BET) method was employed to determine the surface area of the scaffolds.

In *vitro* degradation

The degradation of specimens was determined by measuring the weight loss in Tris-HCl solution at different time points. Briefly, the specimens were immersed in Tris-HCl solution with a weight-to-volume ratio of 0.2 g mL^{-1} under continuous shaking at 37 °C. At each time point, the specimens was cleaned with deionized water,

RSC Advances Accepted Manuscript

This journal is © The Royal Society of Chemistry 2012

dried at 60 °C overnight, and weighed. Then the specimens were re-immersed in a fresh Tris-HCl solution with the same weight-to-volume ratio under continuous shaking at 37 °C. The test period for degradation continued for 90 days. The weight loss was calculated as the percentage of the initial specimen weight.
The degradation was also analyzed by monitoring the ion concentrations of calcium (Ca) and phosphorous (P) in Tris-HCl solution using an inductively coupled plasma atomic emission spectroscopy (ICP-AES, IRIS 1000, Thermo Elemental, USA).

Protein adsorption
Fibronectin (FN)/PBS (10 μg mL^{-1}) was used to study the protein adsorption on scaffolds. Scaffolds were immersed in FN/PBS solution for 4 h in a cell incubator. Afterwards, the scaffolds were rinsed with PBS for 6 times to remove unabsorbed proteins and immersed in 500 μL of 1% sodium dodecyl sulfate (SDS) solution for 1 h (5 times) to collect proteins absorbed on scaffolds. The concentrations of FN in SDS solution were determined using an ELISA plate reader (ELx 800, BIO-TEK) and a MicroBCA protein assay kit (Pierce, Rockford, IL, USA).

MC3T3-E1 cell culture
The mouse MC3T3-E1 cells (subclone 4, ATCC CRL-2593) were cultured in the same way as reported previously.[7-9, 22-24] Scaffolds were rinsed in 70% alcohol solution for ~3 times, sterilized by 70% alcohol solution for 5 × 30 min under shaking, and dried completely under reduced pressure at 60 ℃ overnight. Cells were seeded on scaffolds at a density of ~12,000 cells per cm^2 in 12-well plates with α-Minimum Essential Media (α-MEM, Gibco) supplemented with 10% fetal bovine serum (Sijiqing, Hangzhou, China) plus 100U mL^{-1} penicillin and 100 μg mL^{-1} streptomycin sulfate in a cell incubator.

MTT assay
The cell attachment and proliferation were analyzed with an MTT assay by quantifying the cell numbers as reported earlier.[22] Briefly, at the time point, the cell culture medium was extracted and the scaffolds were rinsed with PBS for ~3 times. Afterwards, 10 μL of MTT (MajorBiochem, Shanghai, China) solution mixed with 100 μL culture medium was added to each well and the cells were incubated in the cell incubator for 4 h. Then 100 μL of SDS-HCl solution was added to each well and mixed thoroughly before incubated for another 4 h. The solution in each well was mixed completely again and 100 μL of each solution was transferred to a 96-well plate. The ELISA plate reader (ELx 800, BIO-TEK) was used to record absorbance at 570 nm. The absorbance was converted to cell numbers using a standard curve according to the manufacturer's manual.

Immunofluorescence microscopy and SEM observation
The cell spreading and adhesion on scaffolds were evaluated by cytoplasma staining and focal adhesion (FA) staining as described previously.[7-9, 22] At day 1 post seeding, the cells were fixed with 4% paraformaldehyde (PFA) solution for ~30 min at room temperature, rinsed with phosphate buffered saline (PBS) for 3 times, and permeabilized with 0.2% (v/v) Triton X-100. Then cells again were rinsed with PBS for 3 times and stained with rhodamine-phalloidin (RP) and mouse monoclonal anti-vinculin antibody (V 9264, Sigma-Aldrich) for 2 h in the cell incubator. The cells were rinsed with PBS for 5 times before labelled with anti-mouse IgG-FITC antibody (F 0257, Sigma) in the cell incubator overnight. The cytoskeleton and focal adhesions (FAs) were observed using confocal laser scanning microscopy (LEICA TCS SD2, Germany) after stained with 4,6-diamidino-2-phenylindole (DAPI) at room temperature. The cell spreading area was measured from ~150 non-overlapping cells using the ImageJ software (National Institutes of Health, Bethesda, MD). At day 1, the cells were treated as described previously for SEM observation.[7,22]

Differentiation
After cultured for 2 weeks, cells were transferred to centrifuge tubes, rinsed with PBS for 3 times, trypsinized, and immersed in α-MEM media (5 mL) under slight shaking. The cells were then collected and washed with PBS solution using centrifugation at 1000 rpm for 2 min. The cell pellet was suspended in 1 ml of 0.2% Nonidet P-40 solution and sonicated at 0 °C for 2 min. An ALP detection kit (Sigma, St. Louis, MO) and a QuantiChrom calcium assay kit (BioAssay Systems, Hayward, CA) were used to determine the ALP activity and calcium content, respectively. The calcium deposition on the scaffolds was stained in the Alizarin red S solution (Ricca Chemical, Arlington, TX) for 30 min, rinsed with deionized water for 5 × 30 min, and photographed with a digital camera.

Gene expression
The expressions of alkaline phosphatase (ALP), osteocalcin (OCN), osteopontin (OPN), and glyceraldehyde-3-phosphate dehydrogenase (GAPDH) utilized for normalization of any differences in amount of total RNA, were measured with real-time polymerase chain reaction (PCR) according to previous reports.[7,22] After cells were cultured for 14 days, the *c*DNA was synthesized using the reverse transcriptase MMLV (Promega, USA) and Oligo$(dT)_{18}$ (Takara, Japan) according to the manual. The oligonucleotide primers for real-time PCR were: GAPDH sense, 5'-ACT TTG TCA AGC TCA TTT CC-3'; GAPDH anti-sense, 5'-TGC AGC GAA CTT TAT TGA TG-3'; ALP sense, 5'-GCC CTC TCC AAG ACA TAT A-3'; ALP anti-sense, 5'-CCA TGA TCA CGT CGA TAT CC-3'; OCN sense, 5'-CAA GTC CCA CAC AGC AGC TT-3'; OCN anti-sense, 5'-AAA GCC GAG CTG CCA GAG TT-3'; OPN sense, 5'-ACA CTT TCA CTC CAA TCG TCC-3'; OPN anti-sense, 5'-TGC CCT TTC CGT TGT TGT CC-3'.

Statistical analysis
Cell studies, ICP-AES measurement, weight loss, gel fraction test, mechanical test, water adsorption measurement, porosity test, and protein adsorption were performed in quadruplicates for each specimen. The data were expressed as mean ± standard deviation. Statistical analysis was performed using one-way ANOVA with post hoc tests. The values of $p < 0.05$ or 0.01 were considered to be significant difference.

Results and Discussion

The morphologies and compositions of CPC, CW-CPC, and CH-CPC scaffolds were verified with SEM and EDS tests as depicted in Figure 1. The SEM images of CPC and CW-CPC scaffolds showed the typical structural features of scaffolds fabricated via the particulate-leaching method, which rendered the scaffolds interconnected macro-pores with a diameter of 400~500 μm (also see Figure S1a). When the breath-figure method was applied to CPC scaffolds as illustrated in Scheme 1, the walls, ridges, and valleys of macro-pores on the CPC scaffold surface were fully covered with honeycomb pores ranging from 1.5 μm to 3.7 μm in diameter as indicated in Figure 1f-h. However, the topography of walls and valleys in scaffolds showed clear difference in pore shape and uniformity. The pores located on the valleys were observed to be more uniform than those on the macro-pore walls and the pore sizes were measured to be 1.8 ± 0.3 μm and 2.5 ± 1.2 μm on the valleys and walls, respectively. During the formation of honeycomb pores via breath-figure method, the surrounding moist air first is condensed onto the polymer solution surface because of the sharp

RSC Advances Accepted Manuscript

temperature drop resulted from the fast evaporation of the volatile organic solvent, here, DCM. Then the condensed water droplets are arranged orderly as templates and the honeycomb pores are formed after the water droplets are removed completely.[7, 9, 25] In this study, the honeycomb pores were fabricated on 3-demensional scaffolds instead of flat substrata, which gave challenge to the stability of arranged water droplets on the walls. The water droplets tended to flow down to the valleys due to gravity and coalesce easily, which might cause the poor pore size uniformity on the walls. Hence, to obtain honeycomb pores, it is critical to apply airflow with high rate for drying the polymer coating on the walls faster. Figure 1h showed the cross-section view of the honeycomb pores on the valley, presenting mono-layer pores on the surface due to the lighter mass density of water droplets than the DCM solvent.[7, 25] To take insight into the pore formation inside the CPC scaffold, we also used SEM to observe the inside as shown in Figure S1b and Figure S1c. Prominently, the honeycomb pores were also formed on the macropores inside the CPC scaffolds, even though not fully, and the regularity of pores was slightly lower than that on the scaffold surface, which might be attributed to the poor airflow inside the scaffolds during fabrication. Meanwhile, the EDS tests were also performed for these scaffolds (Figure 1i-k), which showed that both CW-CPC and CH-CPC scaffolds contained carbon element assigned to PLLATA polymer, whereas CPC scaffolds only had the typical Ca, P, and O elements. The gel fractions for CW-CPC and CH-CPC scaffolds were measured to be 86 ± 3% and 88 ± 4%, respectively, meaning that both formed great networks initiated by UV light. Herein, we might make a short conclusion according to literatures and our studies that the formation of honeycomb pores via breath-figure method on 3-dimensional structure requires the following conditions. The airflow is indispensable to trigger faster evaporation of polymer solution and stabilize the honeycomb pores more efficiently. Besides, the 3-dimensional structure has to be insoluble in the organic solvent used for dissolving polymers, otherwise, the water droplet could not be stabilized as expected.

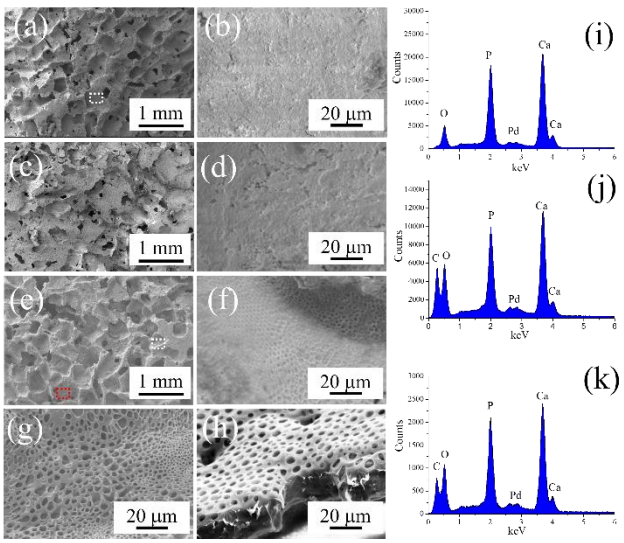

Figure 1. SEM images of (a, b) CPC, (c, d) CW-CPC, and (e-h) CH-CPC scaffolds. (b, d) shows the enlarged area of the white rectangle, (f-h) show the view of the macro-pore valley (white rectangle in (e)), wall (red rectangle in (g)), and the cross-section of the valley. Representative EDS spectra of (i) CPC, (j) CW-CPC, and (k) CH-CPC scaffolds.

The chemical compositions of CPC, CW-CPC, and CH-CPC scaffolds were further characterized with XRD and TGA tests (Figure 2a and b). The CPC powders composed of reactive ingredients of tetracalcium phosphate (TTCP, $Ca_4(PO_4)_2O$) and dicalcium phosphate anhydrous (DCPA, $CaHPO_4$) in an equivalent molar ratio were purchased from Shanghai Rebone Biomaterials Co., Ltd and the cement setting can be expressed as the following equation (1).

$$2Ca_4(PO_4)_2O + 2CaHPO_4 \longrightarrow Ca_{10}(PO_4)_6(OH)_2\ (HA) \qquad (1)$$

The XRD patterns of CPC, CW-CPC, and CH-CPC scaffolds showed the same indices corresponding to the diffraction peaks of HA (JCPDS~03-0690) and the residuals of TTCP (JCPDS~25-1137) as reported previously, [26] indicating that the XRD method could not detect the PLLATA crystals due to the low composition. Nonetheless, TGA curves demonstrated the precise weight composition of PLLATA polymer in CW-CPC and CH-CPC scaffolds as shown in Figure 2b. When the heating temperature was higher than 100 °C, the water residue started to be removed. The PLLATA polymer started to degrade when the temperature was higher than 300 °C.[27] The weight percentages of the PLLATA polymer in CW-CPC and CH-CPC scaffolds were measured to be 5% and 3.0%, respectively. The slightly higher weight percentage of PLLATA polymer in CW-CPC scaffolds compared with CH-CPC scaffolds might be attributed to the airflow, resulting in extra loss of polymer solution in scaffolds during fabrication.

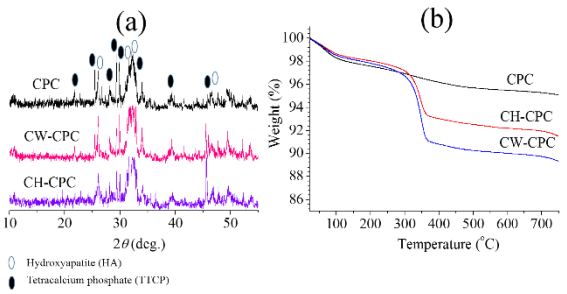

Figure 2. (a) XRD patterns and (b) TGA curves of CPC, CW-CPC, and CH-CPC scaffolds.

The PLLATA coating on CPC scaffolds influenced the physical properties, such as compressive strength, porosity, surface area, and water adsorption (Table 1). The crosslinked coating without honeycomb pores (CW-CPC) enhanced the compressive strength from 1.6 ± 0.2 MPa for CPC scaffolds to 2.1 ± 0.1 MPa for CW-CPC scaffolds. The formation of honeycomb pores in crosslinked coating (CH-CPC), however, lowered the compressive strength to 2.0 ± 0.2 MPa, still higher than that for CPC scaffolds. We also tested the compressive strength for PLLATA coated CPC with or without honeycomb pores, but without crosslinked networks (H-CPC and W-CPC, respectively), which were 1.6 ± 0.4 MPa and 1.6 ± 0.2 MPa, respectively. The improved compressive strength for CW-CPC and CH-CPC over W-CPC and H-CPC should be attributed to the formation of crosslinked networks. Accordingly, the porosities of the CW-CPC and CH-CPC scaffolds were decreased due to the PLLATA coating occupying pore volume on scaffolds. Interestingly, the surface area of scaffolds increased dramatically from ~37 $m^2\ g^{-1}$ for CPC or CW-CPC to ~62 $m^2\ g^{-1}$ for CH-CPC due to the honeycomb pores available inside. Similarly, the water

RSC Advances Accepted Manuscript

This journal is © The Royal Society of Chemistry 2012

adsorption was also improved greatly for CH-CPC scaffolds compared with CPC or CW-CPC ones.

Table 1. Physical characterizations and protein adsorption of scaffolds

Scaffolds	Compressive strength (MPa)	Porosity (%)	Surface area (m^2 g^{-1})	Water adsorption (%)	Protein adsorption (μg cm^{-2})
CPC	1.6 ±0.2	75 ±8	37 ±5	41 ±6	4.2 ±0.5
CW-CPC	2.1 ±0.1	54 ±7	35 ±11	38 ±4	6.1 ±1.3
CH-CPC	2.0 ±0.2	53 ±3	62 ±14	48 ±5	8.4 ±1.2

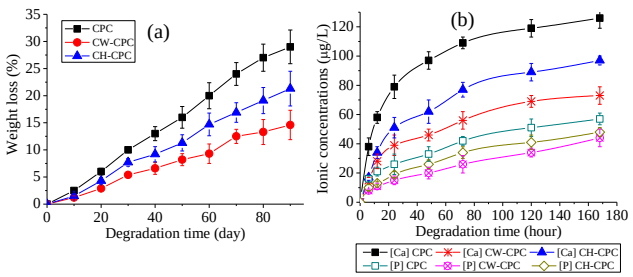

Figure 3. Degradation of CPC, CW-CPC, and CH-CPC scaffolds: (a) weight loss in Tris-HCl solution at different time points. (b) Ionic concentrations of Ca and P in Tris-HCl solution at different time points.

To evaluate the potential of scaffolds for bone regeneration, it is of importance to study their degradation kinetics.[2] Thereby, the in *vitro* degradation ability was investigated in terms of weight loss and the ion release in Tris-HCl solution as shown in Figure 3. All scaffolds showed increasing weight loss with time, indicating biodegradation ability (Figure 3a). However, compared with CPC scaffolds, the degradation rates of CW-CPC and CH-CPC were lowered by the PLLATA coating. As demonstrated earlier that PLLA showed extremely slow degradation,[28] even though considered as a biodegradable polymer both in *vitro* and in *vivo*. Thus, the slower degradation of PLLATA coating than that of CPC scaffolds might inhibit the ion release from CW-CPC and CH-CPC. More importantly, the CH-CPC displayed faster weight loss than CW-CPC, which might be attributed to the fact that honeycomb pores provided more efficient ion penetration from CPC scaffolds than solid coating on CW-CPC scaffolds. There are several potential factors contributing to the good degradation of CPC scaffolds. First, the acidic condition in degradation solution could increase the HA dissolution rate easily. Second, the high surface area the degradation solution contacted might further promote the dissolution of CPC scaffolds. Third, the mechanically weak porous samples partially disintegrated during shaking over 90 days and lost weight by losing particulate fragments, which might also provide an explanation why the PLLATA coated CPC lost less weight since the PLLATA mechanically stabilized the scaffolds (Table 1). Figure 3b further confirmed the ion release from scaffolds during degradation. Consistently, the Ca and P ions released faster from CPC scaffolds than others and the CW-CPC scaffolds showed the slowest ion release. Apparently, the CH-CPC scaffolds had good biodegradation ability, even though the degradation was slightly slower than CPC scaffolds.

RSC Advances Accepted Manuscript

RSC Advances RSCPublishing

ARTICLE

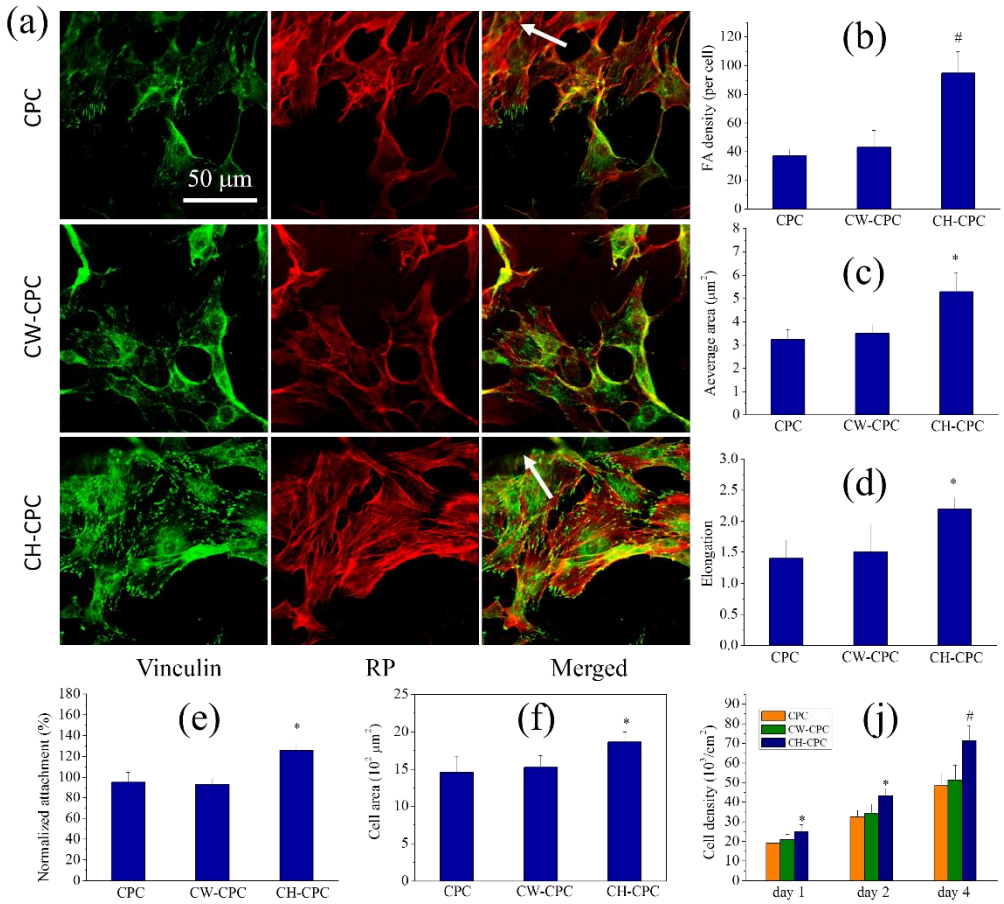

Figure 4. (a) Fluorescent images of MC3T3-E1 cells stained with vinculin (left column, green) and RP (middle column, red), and merged images (right column) at day 1 post seeding with white arrow heads indicating the area out of phase. Scale bar of 50 μm is applicable to all images. (b) Density, (c) average area, and (d) elongation of FAs. (e) Cell attachments determined by the MTT assay on CPC, CW-CPC, and CH-CPC scaffolds, normalized to tissue culture plates. (f) Average cell area on CPC, CW-CPC, and CH-CPC scaffolds at day 1 post seeding. (j) Cell proliferation represented by cell numbers determined by the MTT assay on CPC, CW-CPC, and CH-CPC scaffolds at day 1, 2, and 4 post seeding. *: $p < 0.05$ and #: $p < 0.01$ are relative to CPC and CW-CPC scaffolds.

The MC3T3-E1 cell functions including cell adhesion, attachment, spreading, and proliferation were investigated as demonstrated in Figure 4. The vinculin-stained images in Figure 4a clearly showed that cells on CH-CPC scaffolds had significantly more green spots, namely, FAs, than on CPC and CW-CPC ones. Because the scaffolds did not have perfect flat surfaces, it was normal to observe the cells out of phase, as indicated by white arrows. The FAs were also quantified with ImageJ software in terms of FA density defined as the average number of FAs per cell, FA area, and elongation of FAs defined as the reciprocal of circularity (Figure 4b-d). All these parameters showed significantly higher values on CH-CPC scaffolds than CPC and CW-CPC ones, indicating better adhesion on CH-CPC scaffolds. In a good agreement, cell attachment tested at 4 h by the MTT assay also demonstrated better cell anchorage on CH-CPC scaffolds than CPC and CW-CPC scaffolds. The cell growth at day 1 was also characterized with SEM observation (Figure S2), clearly showing that cells could grow into the macropores on all samples and the cells spread better inside the macropores of CH-CPC scaffolds. Meanwhile, the RP-stained images in Figure 4a also indicated that cells on CH-CPC scaffolds had larger spreading area than CPC and CW-CPC ones, which was also confirmed by quantification with ImageJ software (Figure 4f) from fluorescent images (Figure S3). The average cell spreading area increased from

RSC Advances Accepted Manuscript

~1,300 μm^2 on CPC or CW-CPC scaffolds to ~1700 μm^2 on CH-CPC scaffolds.

Thus, the MC3T3-E1 cell attachment, adhesion, spreading, and proliferation on CPC and CW-CPC scaffolds did not show significant differences, but were not comparable to those on CH-CPC scaffolds. It is reasonable to conclude that the honeycomb pores benefited the MC3T3-E1 cell behavior on CH-CPC scaffolds. Cells, especially anchorage-dependent cell lines, strongly respond and react to micro or nanotopography via the "contact guidance" effect.[6-9, 12, 25] For instance, fibroblasts were observed to preferentially stay on the ridges of microgrooves in an oriented manner and the actin filaments were launched from the FA points, the alignment of which triggered the corresponding orientation of actin filaments or stress fibers.[7, 12, 29] Honeycomb pores, as reported previously, play great roles in regulating cell functions.[7, 9, 22, 30] The influence of honeycomb pores on cell behavior, to date, has been attributed to several aspects. First, honeycomb pores can promote the adsorption of extracellular matrix (ECM) proteins including fibronectin (FN), which supply integrin receptors for cellular anchorage at the very early stage and further manipulate cellular events, such as attachment, adhesion, proliferation, and differentiation.[6, 7, 9, 11] In this study, the topographical influence on FN adsorption was also evaluated as shown in Table 1. The CW-CPC scaffolds presented significantly higher FN adsorption than CPC scaffolds, even though they had the similar surface area which was believed to have linear relationship with protein adsorption.[7] However, the PLLATA coating in CW-CPC scaffolds changed the surface property which directly guided protein-surface interaction. It is believed that hydrophilic surfaces lower the protein adsorption, whereas hydrophobic ones benefit the protein adsorption.[22, 31] As known, PLLATA is a much more hydrophobic material than CPC. Consequently, the PLLATA polymer coating might enhance the FN deposition on CW-CPC scaffolds. More interestingly, the FN adsorption strongly increased from 6.1 ± 1.3 μg cm^{-2} on CW-CPC scaffolds to 8.4 ± 1.2 μg cm^{-2} on CH-CPC scaffolds, which should be attributed to the pores, providing larger contact surface area for FN deposition. The FAs, namely, the complex of cytoskeleton-adapter protein-integrin which is the transmembrane heterodimers of the α-subunit and β-subunit, regulate cell functions through "inside-out-signaling" between cells and ECM and "outside-in-signaling" between biomaterial surface and integrin receptors.[32] Besides, the fibril-like aggregates of FN on the periphery of pores, observed previously,[33-36] which were believed to influence the formation of FAs, might also work here, even though they were not demonstrated in this study. Therefore, the protein adsorption on these scaffolds might provide a reasonable explanation for cell attachment, adhesion, and proliferation. Second, the formation of honeycomb pores generated a large region of junction or discontinuity, which provided favorable microenvironment for cell adhesion and growth. Previous investigation on the regulation of MC3T3-E1 cells on honeycomb films prepared via breath-figure method also demonstrated that honeycomb pores provided more junction or discontinuity for cell anchorage than flat films, inducing better cell response.[7, 9] Last but not least, the slow release of Ca and P ions from scaffolds, as demonstrated earlier, played a subtle role in enhancing cell functions. Extracellular signal-regulated kinases (ERKs), the family member of mitogen-activated protein kinases (MAPK), have been believed to be crucial for regulating osteoblast functions, including adhesion, spreading, migration, integrin expression, and mineralization.[37] The cellular Ca ion was demonstrated to be involved in ERK ½ activation in osteoblasts.[22] Earlier findings suggested that Ca ion significantly tuned ALP activity and mineralization of MC3T3-E1 cells and the Ca ions up-regulated the expression of TGF-1 in osteoblastic cells.[38-40] On the other hand, P ions are also believed to function as a specific signal for skeletal cells, which influences cell proliferation, mineralization, and apoptosis. So, the Ca and P ions collaborated to promote cell adhesion, proliferation, and even differentiation. However, all scaffolds could release both Ca and P ions gradually as demonstrated by ICP test and the concentrations of Ca and P ions for CH-CPC sample were even lower than for CPC and CW-CPC samples, meaning that the Ca and P ions should not be the reason why the cell functions were enhanced on CH-CPC scaffolds compared with other scaffolds.

The MC3T3-E1 cell differentiation was also studied by quantifying ALP activity and Ca content (Figure 5a), Alizarin red S staining (Figure 5b), and the expression levels of osteogenesis-related markers ALP, OCN, and OPN. Apparently, ALP activity and Ca content, were greatly promoted on CH-CPC scaffolds, whereas there was no significant difference between CPC and CW-CPC scaffolds. This was further confirmed by Alizarin red S staining that the cells on CH-CPC scaffolds presented the deepest color intensity among them, indicating the best calcium deposition on CH-CPC scaffolds. Consistently, the ALP, OCN, and OPN showed significantly higher expression levels on CH-CPC scaffolds than on CPC or CW-CPC scaffolds. Even though the Ca and P ions released from scaffolds might be helpful for MC3T3-E1 cell differentiation as discussed above, it does not provide reasonable understanding to interpret the enhanced MC3T3-E1 cell differentiation on CH-CPC scaffolds since the CPC scaffolds could release more Ca and P ions. Another proper explanation for cell differentiation is that the cells on CH-CPC scaffolds proliferated faster than on the other scaffolds and reached confluence earlier to launch cell differentiation, which results in the best differentiation on CH-CPC scaffolds among all scaffolds.

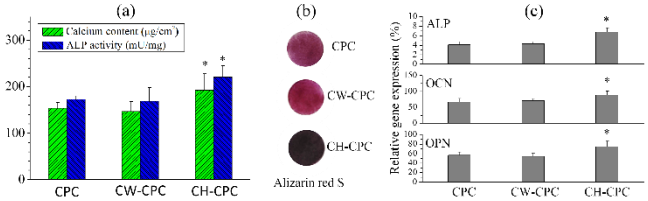

Figure 5. Cell differentiation on CPC, CW-CPC, and CH-CPC scaffolds. (a) Calcium content and ALP activity quantified by a QuantiChrom calcium assay kit and an ALP detection kit, respectively. *: $p < 0.05$ is relative to CPC and CW-CPC scaffolds. (b) Alizarin red S staining for calcium deposition. Deeper intensity indicated better differentiation. (c) Gene expression levels of ALP, OCN, and OPN relative to GAPDH at day 14 on CPC, CW-CPC, and CH-CPC scaffolds. *: $p < 0.05$ relative to others.

Conclusions

In this study, we for the first time reported the fabrication of photo-crosslinked hierarchically honeycomb-patterned calcium phosphate cement scaffolds (CH-CPC) via the breath-figure method. The CH-CPC scaffold surface were fully covered with a mono-honeycomb layer and the inside of the scaffold was also covered with pores, but with lower regularity in pore size. The crosslinked networks in CW-CPC and CH-CPC scaffolds enhanced their compressive strength. The surface area and water adsorption in CH-CPC scaffolds were greatly enhanced compared with CPC and CW-CPC scaffolds due to the formation of honeycomb pores, which also promoted the FN adsorption. More importantly, the MC3T3-E1 cell adhesion, spreading, proliferation, and differentiation were also strongly

RSC Advances Accepted Manuscript

enhanced on CH-CPC scaffolds. The method in this study for developing honeycomb-patterned 3-dimensional CPC scaffolds, undoubtedly, provides an efficient technology to prepare more advanced scaffolds for bone regeneration.

Acknowledgements

This study was supported by grants from the National Natural Science Foundation of China (31271031, C100302), the International Cooperation Project of the Ministry of Science and Technology of China (2013DFB50280).

Notes and references

[a] Department of Biomedical Engineering, Case Western Reserve University, Cleveland, OH 44106, USA.

[b] Key Laboratory for Ultrafine Materials of Ministry of Education, East China University of Science and Technology, Shanghai 200237, P.R China.

[c] College of Physical Science and Technology, Sichuan University, Chengdu 610041, China

[d] Department of Orthopaedics Trauma, Changhai Hospital, Second Military Medical University, Shanghai 200433, China

*Corresponding author. E-mail address: qianjun@ecust.edu.cn (J Qian); biomaterbone@163.com (J.C.Su)

1. Y. Khan, M. J. Yaszemski, A. G. Mikos and C. T. Laurencin, *J. Bone and Joint Surg. Am*, 2008, **90A**, 36.
2. J. Wei, X. Wu, C. Liu, J. Jia, S. j. Heo, S. E. Kim, Y. T. Hyun and J. W. Shin, *J. Am. Ceram. Soc*, 2009, **92**, 1017.
3. J. Wei, J. F. Jia, F. Wu, S. C. Wei, H. J. Zhou, H. B. Zhang, J. W. Shin and C. S. Liu, *Biomaterials*, 2010, **31**, 1260.
4. N. Bolgen, Y. Yang, P. Korkusuz, E. Guzel, A. J. El Haj and E. Piskin, *Tissue. Eng. Part A*, 2008, **14**, 1743.
5. H. Guo, J. C. Su, J. Wei, H. Kong and C. S. Liu, *Acta Biomater.*, 2009, **5**, 268.
6. C. J. Bettinger, R. Langer and J. T. Borenstein, *Angew. Chem. Int. Ed.*, 2009, **48**, 5406.
7. X. Wu and S. Wang, *ACS Appl. Mater. Interfaces*, 2012, **4**, 4966.
8. X. Wu and S. Wang, *Adv. Healthcare Mater.*, 2013, **2**, 326.
9. X. Wu and S. Wang, *Polymer*, 2014, **55**, 1756.
10. R. Ye and D. G. Hayes, *Biocatal. Biotransform*, 2012, **30**, 209.
11. R. G. Flemming, C. J. Murphy, G. A. Abrams, S. L. Goodman and P. F. Nealey, *Biomaterials*, 1999, **20**, 573.
12. K. Anselme and M. Bigerelle, *Int. Mater. Rev.*, 2011, **56**, 243.
13. X. Wu, L. Ye, K. Liu, W. Wang, J. Wei, F. Chen and C. Liu, *Biomed. Mater.*, 2009, **4**, 045008.
14. R. Ye and F. Harte, *J. Dairy Sci.*, 2013, **96**, 799.
15. L. A. Connal, *Aust. J. Chem.*, 2007, **60**, 794.
16. L. A. Connal and G. G. Qiao, *Soft Matter*, 2007, **3**, 837.
17. L. A. Connal, R. Vestberg, P. A. Gurr, C. J. Hawker and G. G. Qiao, *Langmuir*, 2008, **24**, 556.
18. L. A. Connal and G. G. Qiao, *Adv. Mater.*, 2006, **18**, 3024.
19. Y. Yang, N. Bajaj, P. Xu, K. Ohn, M. D. Tsifansky and Y. Yeo, *Biomaterials*, 2009, **30**, 1947.
20. N. Nasongkla, X. Shuai, H. Ai, B. D. Weinberg, J. Pink, D. A. Boothman and J. M. Gao, *Angew. Chem. Int. Ed.*, 2004, **43**, 6323.
21. K. Wang, L. Cai, L. Zhang, J. Y. Dong and S. F. Wang, *Adv. Healthcare Mater.*, 2012, **1**, 292.
22. X. H. Wu, Z. Y. Wu, J. C. Su, Y. G. Yan, B. Q. Yu, J. Wei and L. M. Zhao, *RSC Adv.*, 2015, **5**, 6607.
23. H. Zhou, J. Wei, X. Wu, J. Shi, C. Liu, J. Jia, C. Dai and Q. Gan, *J. Mater. Sci.: Mater. Med.*, 2010, **21**, 2175.
24. H. Zhou, X. Wu, J. Wei, X. Lu, S. Zhang, J. Shi and C. Liu, *J. Mater. Sci.: Mater. Med.*, 2011, **22**, 731.
25. U. H. F. Bunz, *Adv. Mater.*, 2006, **18**, 973.
26. M. Alshaaer, M. H. Kailani, H. Jafar, N. Ababneh and A. Awidi, *Adv. Mater. Sci. Eng.*, 2013, **2013**, 8.
27. H. M. Chen, X.C. Du, A.S. Yang, J.H. Yang, T. Huang, N. Zhang, W. Yang, Y. Wang and C. L. Zhang, *RSC Adv.*, 2014, **4**, 3443.
28. V. Arias, A. Höglund, K. Odelius and A. C. Albertsson, *Biomacromolecules*, 2014, **15**, 391.
29. M. J. Dalby, *Med. Eng. Phys.*, 2005, **27**, 730.
30. M. Tanaka, *Biochim. Biophys. Acta*, 2011, **1810**, 251.
31. R. D. K. Misra, W. W. Thein-Han, T. C. Pesacreta, K. H. Hasenstein, M. C. Somani and L. P. Karjalainen, *Acta Biomater.*, 2009, **5**, 1455.
32. K. Anselme, *Biomaterials*, 2000, **21**, 667.
33. J. R. McMillan, M. Akiyama, M. Tanaka, S. Yamamoto, M. Goto, R. Abe, D. Sawamura, M. Shimomura and H. Shimizu, *Tissue Eng.*, 2007, **13**, 789.
34. H. Sunami, E. Ito, M. Tanaka, S. Yamamoto and M. Shimomura, *Colloid Surf., A*, 2006, **284**, 548.
35. S. Yamamoto, M. Tanaka, H. Sunami, K. Arai, A. Takayama, S. Yamashita, Y. Morita and M. Shimomura, *Surf. Sci.*, 2006, **600**, 3785.
36. S. Yamamoto, M. Tanaka, H. Sunami, E. Ito, S. Yamashita, Y. Morita and M. Shimomura, *Langmuir*, 2007, **23**, 8114.
37. A. Curtis and C. Wilkinson, *Biomaterials*, 1997, **18**, 1573.
38. A. Lazary, B. Balla, J. P. Kosa, K. Bacsi, Z. Nagy, I. Takacs, P. P. Varga, G. Speer and P. Lakatos, *Biomaterials*, 2007, **28**, 393.
39. H. Matsuoka, H. Akiyama, Y. Okada, H. Ito, C. Shigeno, J. Konishi, T. Kokubo and T. Nakamura, *J. Biomed. Mater. Res.*, 1999, **47**, 176.
40. X. Wu, J. Wei, X. Lu, Y. Lv, F. Chen, Y. Zhang and C. Liu, *Biomed. Mater.*, 2010, **5**, 035006.

RSC Advances Accepted Manuscript

 This journal is © The Royal Society of Chemistry 2012